An explicit integration scheme for hypo-elastic viscoplastic crystal plasticity

K. ZHANG[1] *, B. HOLMEDAL[1], S. DUMOULIN[2], O.S. HOPPERSTAD[3,4]

[1] **Department of Materials Science and Engineering, Norwegian University of Science and Technology, NO-7491 Trondheim, Norway**

[2] **SINTEF Materials and Chemistry, NO-7465 Trondheim, Norway**

[3] **Department of Structural Engineering, Norwegian University of Science and Technology, NO-7491 Trondheim, Norway**

[4] **Structural Impact Laboratory (SIMLab), Center for Research-based Innovation, Norwegian University of Science and Technology, NO-7491 Trondheim, Norway**

Abstract: An explicit integration scheme for rate-dependent crystal plasticity (CP) has been developed in this work. Additive decomposition of the velocity gradient tensor into lattice and plastic parts is adopted for describing the kinematics; the Cauchy stress is calculated by using a hypo-elastic formulation, applying the Jaumann stress rate. This CP scheme has been implemented into a commercial finite element code (CPFEM). Uniaxial compression and rolling processes were simulated. The results show good accuracy and reliability of the integration scheme. The results were compared to simulations using one hyper-elastic CPFEM implementation which involves multiplicative decomposition of the deformation gradient tensor. It is found that the hypo-elastic implementation is only slightly faster and has a similar accuracy as the hyper-elastic formulation.

Keywords: crystal plasticity; hypo-elasticity; hyper-elasticity; forward Euler integration

1. Introduction

Crystal plasticity (CP) models originate from the physical aspect of plastic deformation, i.e. slip dominated plastic deformation [1]. Constitutive laws of single crystals together with homogenization methods across polycrystalline aggregates define the polycrystal plasticity model [2, 3]. Mechanical properties, texture evolution and other material phenomena can be simulated using CP models [2-5]. The main inputs into CP models are initial texture and material parameters.

One key component of a crystal plasticity model at single grain level is the determination of shear strains or shear strain rates on slip systems, which can generally be solved using two different approaches, either rate-independent or rate-dependent. For the rate-independent method, the shear strain is determined to accommodate the prescribed plastic deformation using a minimum dissipation energy assumption [1]. Only the slip systems for which the resolved shear stress equals the critical resolved shear stress are considered to be active. It can be implemented numerically by solving linear equations or using e.g. the Simplex method with high computational efficiency [6].

Corresponding author: K. ZHANG, Tel.: +47-73594004. E-mail: kai.zhang@ntnu.no

However, due to the Taylor ambiguity, an additional criterion is needed [7]. The rate-dependent crystal plasticity (RDCP) model assumes that all slip systems are active and uses a viscoplastic flow rule. Although without Taylor ambiguity, RDCP could lead to numerical instabilities of integration, because most metals exhibit a weak rate dependence at room temperature [8]. Since first introduced by PEIRCE et al [9], the crystal plasticity theory implemented in the finite element method (CPFEM) has matured into a whole family of constitutive and numerical formulations that have been applied to a broad variety of crystal mechanical problems [3]. CPFEM has both theoretical and practical advantages. First, grains are represented by single or multiple elements while both stress equilibrium and strain compatibility can be fulfilled at boundaries. Second, complex boundary conditions are easily specified in the FEM code. Hence, CPFEM is applicable to simulations of engineering processes. The main drawback of CPFEM is the huge computational cost and the numerical instabilities [2]. Thus, robust and efficient integration schemes are required to reduce computational cost and improve the stability [2, 8, 10-14].

DUMOULIN et al [2] implemented and evaluated three different integration schemes for RDCP, including two forward Euler methods and one implicit integration method. Multiplicative decomposition of the deformation gradient tensor $\mathbf{F}$ was used to describe the kinematics and a hyper-elastic formulation was used for the calculation of the Cauchy stress. Rotation of the crystal lattice was obtained by polar decomposition of the elastic deformation gradient tensor $\mathbf{F}^e$. Among those three integration methods, the forward Euler integration scheme proposed by GRUJICIC and BATCHU (GB) [14] proved to be stable, accurate and the fastest. The RDCP model together with the GB forward Euler integration scheme has also been implemented into a commercial finite element code, LS-DYNA [15], via a user defined subroutine UMAT. This model implementation is referred to as hyper-CPFEM in the following since hyper-elasticity is assumed.

In the current work, a new explicit integration scheme for rate-dependent viscoplastic crystal plasticity has been developed. Different from the constitutive models employed by DUMOULIN et al [2], additive decomposition of the velocity gradient tensor $\mathbf{L}$ is employed for the kinematics; hypo-elasticity is assumed for the material and Jaumann stress rate is applied. In the crystal plasticity theory, the hyper- and hypo- elastic formulations should give the same results in terms of the plastic deformation. There is small difference in the elastic part while details about the hypo-elastic and hyper-elastic theories can be found in the literature [16]. The hypo-elastic theory is commonly applied in the continuum plasticity for metals and alloys due to their small elastic strains. Compared with the hyper-elastic crystal plastic framework, the hypo-elastic counterpart has a simpler mathematical formulation and is easier to implement. Hence, the hypo-elastic crystal plasticity model has a potential to speed up the calculations. However, the accuracy and reliability of stress calculation and texture prediction should be evaluated due to the different formulation employed.

The kinematics, kinetics and crystal plasticity models are described in section 2. A new explicit integration scheme is proposed in section 3. The RDCP model has been implemented into LS-DYNA and is termed hypo-CPFEM in the following. The accuracy and efficiency of this new integration scheme are evaluated through numerical simulations and a comparison with the hyper-CPFEM which are shown in section 4, while general conclusions are made in section 5.

2. Kinematics and crystal plasticity models

The model employed in this work is briefly given here while more details can be found in the literature [17, 18]. It includes anisotropic elastic deformation and assumes that all plastic deformation occurs via dislocation slip on {111} <110> crystallographic systems for face centred cubic (FCC) crystal metals.

2.1. Kinematics

All the equations described in the following are formulated in the initial crystal frame unless specified otherwise. The imposed velocity gradient $\mathbf{L}$ can be additively decomposed into symmetric and skew-symmetric parts:

$$\mathbf{L} = \mathbf{D} + \mathbf{W} \tag{1}$$

where $\mathbf{D}$ is the symmetric deformation rate tensor and $\mathbf{W}$ is the skew-symmetric spin tensor. Deformation of single crystals has been attributed to a combination of plastic flow due to crystallographic slips and lattice distortion. Lattice distortion includes elastic distortion and rigid body rotation of the crystal lattice. Thus, for single crystals, the deformation rate $\mathbf{D}$ and spin $\mathbf{W}$ can be further decomposed into lattice and plastic parts as follows:

$$\mathbf{D} = \mathbf{D}^e + \mathbf{D}^p \tag{2}$$

$$\mathbf{W} = \mathbf{W}^* + \mathbf{W}^p \tag{3}$$

where $\mathbf{D}^e$ represents the elastic deformation rate of the lattice, while $\mathbf{D}^p$ is the plastic deformation rate caused by crystallographic slip. $\mathbf{W}^*$ represents the lattice rigid spin, while $\mathbf{W}^p$ is the spin due to slip activities. $\mathbf{D}^p$ and $\mathbf{W}^p$ can be expressed by the shear rates $\dot{\gamma}^s$ on all slip systems:

$$\mathbf{D}^p = \sum_{s=1}^{12} \dot{\gamma}^s \mathbf{P}^s \tag{4}$$

$$\mathbf{W}^p = \sum_{s=1}^{12} \dot{\gamma}^s \mathbf{\Omega}^s \tag{5}$$

with

$$\mathbf{P}^s = \frac{1}{2}(\mathbf{m}^s \otimes \mathbf{n}^s + \mathbf{n}^s \otimes \mathbf{m}^s) \tag{6}$$

$$\mathbf{\Omega}^s = \frac{1}{2}(\mathbf{m}^s \otimes \mathbf{n}^s - \mathbf{n}^s \otimes \mathbf{m}^s) \tag{7}$$

where $\mathbf{m}^s$ is the unit vector defining slip direction, while $\mathbf{n}^s$ is the unit slip plane normal vector, for the slip system s (where $s = 1 - 12$ for FCC metals). $\mathbf{m}^s$ and $\mathbf{n}^s$ are not affected by crystallographic slip but will be rotated by the lattice spin $\mathbf{W}^*$ as:

$$\dot{\mathbf{m}}^s = \mathbf{W}^* \cdot \mathbf{m}^s \tag{8}$$

$$\dot{\mathbf{n}}^s = \mathbf{W}^* \cdot \mathbf{n}^s \tag{9}$$

2.2. Kinetics

The resolved shear stress τ^s on the slip system s can be expressed as:

$$\tau^s = \mathbf{\sigma} : \mathbf{P}^s \tag{10}$$

where $\mathbf{\sigma}$ is the Cauchy stress tensor. For rate-dependent crystal plasticity, the shear rate on slip systems is often calculated using a power-law type equation:

$$\dot{\gamma}^s = \dot{\gamma}_0 \cdot \mathrm{sgn}(\tau^s) \cdot \left| \frac{\tau^s}{g^s} \right|^{\frac{1}{m}} \tag{11}$$

where $\dot{\gamma}_0$ is a reference shearing rate, m is the instantaneous strain rate sensitivity and g^s represents the slip resistance which evolves during the plastic deformation of single grains. The evolution laws of g^s or hardening models will be discussed in section 2.3.

During distortion of single crystals, a coordinate system attached to the lattice will co-rotate with the lattice. The co-rotational lattice frame is related to the fixed lattice frame by a rotation tensor $\mathfrak{R}$ which is orthogonal and updated by the lattice spin tensor $\mathbf{W}^*$:

$$\dot{\mathfrak{R}} = \mathbf{W}^* \mathfrak{R} \tag{12}$$

In the co-rotational frame, Hooke's law can be expressed in the rate form as:

$$\dot{\hat{\mathbf{\sigma}}} = \hat{\mathbf{C}} : \hat{\mathbf{D}}^e \tag{13}$$

where $\hat{\mathbf{C}}$ is a fourth-order elastic modulus tensor and $\hat{\mathbf{D}}^e$ is the elastic deformation rate tensor, both in the co-rotational frame. The fourth-order tensor $\hat{\mathbf{C}}$ accounts for the elastic anisotropy of the cubic lattice. It is assumed to be invariant to plastic deformation and is kept constant in the co-

rational lattice frame. Expressed in the orthonormal basis associated with the crystal lattice, it reads (in Voigt notation):

$$\hat{\mathbf{C}} = \begin{bmatrix} c_{11} & c_{12} & c_{12} & 0 & 0 & 0 \\ c_{12} & c_{11} & c_{12} & 0 & 0 & 0 \\ c_{12} & c_{12} & c_{11} & 0 & 0 & 0 \\ 0 & 0 & 0 & c_{44} & 0 & 0 \\ 0 & 0 & 0 & 0 & c_{44} & 0 \\ 0 & 0 & 0 & 0 & 0 & c_{44} \end{bmatrix} \tag{14}$$

where c_{11}, c_{12} and c_{44} are three independent elastic constants. $\hat{\mathbf{D}}^e$ can be computed by transforming $\mathbf{D}^e$ from the fixed lattice frame to the co-rotational frame as:

$$\hat{\mathbf{D}}^e = \mathfrak{R}^T \mathbf{D}^e \mathfrak{R} \tag{15}$$

where the upper script T means transpose of a tensor or matrix. Then Jaumann stress rate, $\boldsymbol{\sigma}^{\nabla J}$, is now defined by transforming $\dot{\hat{\boldsymbol{\sigma}}}$ into the fixed coordinate system:

$$\boldsymbol{\sigma}^{\nabla J} = \mathfrak{R}\dot{\hat{\boldsymbol{\sigma}}}\mathfrak{R}^T \tag{16}$$

Finally, the material time derivative of the stress tensor is obtained:

$$\dot{\boldsymbol{\sigma}} = \boldsymbol{\sigma}^{\nabla J} + \mathbf{W}^*\boldsymbol{\sigma} - \boldsymbol{\sigma}\mathbf{W}^* \tag{17}$$

2.3. Hardening model

Material hardening is captured at slip system level through g^s in Eq. (11). The hardening law used in this work assumes that the critical resolved shear stress, g^s, initially equals g_0, evolves through:

$$\dot{g}^s = \sum_{n=1}^{12} h^{sn} \left| \dot{\gamma}^n \right| \tag{18}$$

where h^{sn} is the instantaneous strain hardening matrix; s and n are indices referring to slip systems. In this work, h^{sn} is described phenomenologically by a saturation-type law [8, 19]:

$$h^{sn} = h_0[q + (1-q)\delta^{sn}][1 - g^n/g_{sat}]^a \, \mathrm{sgn}[1 - g^n/g_{sat}] \tag{19}$$

where $\delta^{sn} = 1$ for $s = n$ and otherwise zero; h_0, g_{sat} and a are material parameters, representing the reference self-hardening coefficient, the saturation values of slip resistance and the hardening exponent, respectively. The parameter q represents latent hardening.

2.4. Update of grain orientations and the texture

5

If the velocity gradient $\mathbf{L}'$ is prescribed in the sample frame, $\mathbf{L}$ in the initial lattice frame is obtained by the transformation

$$\mathbf{L} = \mathbf{Q}_0 \mathbf{L}' \mathbf{Q}_0^T \tag{20}$$

where the transformation matrix $\mathbf{Q}_0$ depends on the Euler angles (φ_1 , Φ , φ_2). The transformation matrix $\mathbf{Q}$ from the global frame to the current co-rotational lattice frame is updated by:

$$\mathbf{Q} = \mathfrak{R}^T \mathbf{Q}_0 \tag{21}$$

Euler angles of single grains during deformation can be calculated from $\mathbf{Q}$ and are used to represent the texture.

3. Integration algorithm

The crystal plasticity model described above has been implemented into LS-DYNA through a user defined material subroutine. The key input includes material parameters and initial grain orientations. Mechanical response and deformation texture can then be predicted.

For the time integration, a fully explicit scheme based on the forward Euler method is adopted. This method is simple, robust but only conditionally stable and requires small time steps. The main steps of the explicit scheme are summarized below, where all variables at time t_n are known and the variables at $t_{n+1} = t_n + \Delta t$ are to be determined.

a) Compute the resolved shear stress τ_n^s on each slip system using Eq. (10)

b) Compute the slip rate $\dot{\gamma}_n^s$ using Eq. (11)

c) Compute $\mathbf{D}_n^p$ and $\mathbf{W}_n^p$ using Eq. (4) and Eq. (5)

d) Compute $\mathbf{D}_n^e$ and $\mathbf{W}_n^*$ using Eq. (2) and Eq. (3), where $\mathbf{D}$ and $\mathbf{W}$ are constant during the current time step

e) Compute the Jaumann stress rate $\boldsymbol{\sigma}_n^{\nabla J}$ using Eq. (13), Eq. (15) and Eq. (16)

f) Compute $\dot{\boldsymbol{\sigma}}_n$ using Eq. (17) and update $\boldsymbol{\sigma}_{n+1}$:

$$\boldsymbol{\sigma}_{n+1} = \boldsymbol{\sigma}_n + \dot{\boldsymbol{\sigma}}_n \cdot \Delta t \tag{22}$$

g) Update $\mathfrak{R}_{n+1}$ using the backward-Euler method:

$$\mathfrak{R}_{n+1} = \left(\mathbf{1} - \mathbf{W}_n^* \cdot \Delta t\right)^{-1} \mathfrak{R}_n \tag{23}$$

h) Update internal variables and update the critical resolved stress g_{n+1}^s using equations described in section 2.3

i) Update slip direction vectors, $\mathbf{m}_{n+1}^s$, and slip plane normal vectors, $\mathbf{n}_{n+1}^s$, using the backward Euler method:

$$\mathbf{m}_{n+1}^s = \left(\mathbf{1} - \mathbf{W}_n^* \cdot \Delta t\right)^{-1} \mathbf{m}_n^s \tag{24}$$

$$\mathbf{n}_{n+1}^s = \left(\mathbf{1} - \mathbf{W}_n^* \cdot \Delta t\right)^{-1} \mathbf{n}_n^s \tag{25}$$

j) Compute $\mathbf{P}_{n+1}^s$ and $\mathbf{\Omega}_{n+1}^s$ from $\mathbf{m}_{n+1}^s$ and $\mathbf{n}_{n+1}^s$ using Eq. (6) and Eq. (7)

k) Update the grain orientation matrix $\mathbf{Q}_{n+1}$ using Eq. (21)

4. Numerical study and discussion

To evaluate the hypo-elastic formulation used here and the integration algorithm proposed in this work, two numerical studies have been conducted. The first one is the simulation of uniaxial compression of OFHC copper with initially random texture while the second one is the texture prediction after rolling of the same material. The hyper-CPFEM model implemented by DUMOULIN et al [2] with the GB integration scheme has also been used for the above simulation cases. Predicted results from the two CPFEM formulations will be compared in order to evaluate their performance in terms of accuracy and efficiency.

The material parameters are given similar values as reported in the work of KALIDINDI et al [18], as shown in Table 1. 1000 random orientations are used to represent the initial texture of the material and the {111} pole figure is shown in Fig. 1. The representative volume (RVE) has a size of $2\text{mm} \times 2\text{mm} \times 2\text{mm}$. The RVE is meshed with 1000 equal-sized 8 integration point solid elements and each element is assigned one orientation and hence represents one grain, as shown in Fig. 2. Mass scaling is used to speed up the simulations with a scaling factor of 10^8. All simulations were performed on a work-station with Intel Xeon E5620 CPU (2.4 GHz) and 12G memory, and 8 threads were used simultaneously for each simulation.

Table 1 Model parameters used in the simulations.

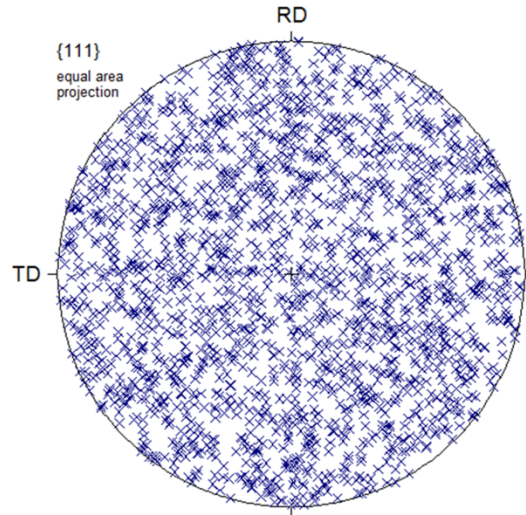| $\dot{\gamma}_0$	m	g_0 (MPa)	g_{sat} (MPa)	h_0 (MPa)	a	q	c_{11} (GPa)	c_{12} (GPa)	c_{44} (GPa)
10^{-3}	0.012	16	148	180	2.25	1.4	186	93	46.5

Fig. 1 Initial {111} equal area pole figure of the 1000 orientations.
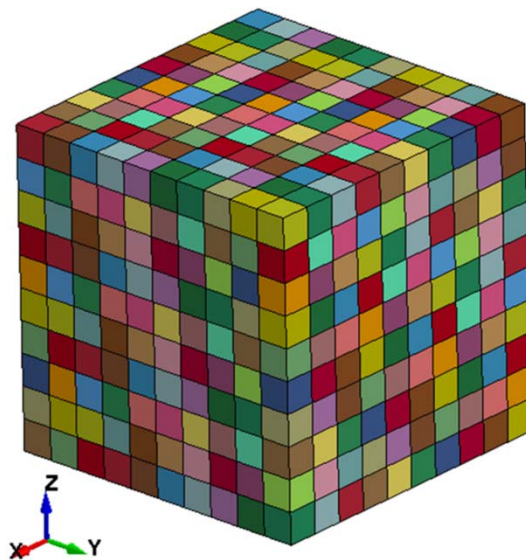

Fig. 2 RVE with 1000 grains.

4.1. Uniaxial compression

The RVE is compressed along the *x*-direction with a speed of 0.01 mm/s to 70% thickness reduction, i.e. the deformation time is 140 seconds. The surfaces along *y*- and *z*- directions are free to move.

The stress-strain curves from simulations using the hypo-CPFEM and the hyper-CPFEM respectively are shown in Fig. 3, where the experimental data from literature [19] is also shown. It can be seen that the hypo-CPFEM and the hyper-CPFEM give the same stress versus strain response. The agreement between the predicted curves and the experiment is reasonable. The CPU

time is shown in Table 2. Both CPFEM models have similar time efficiency, but the hypo-CPFEM is slightly faster.

The good agreement between the predictions by the two CPFEM models validates accuracy and reliability of the crystal plasticity formulations as well as the integration method used for the hypo-CPFEM. Moreover, the fact that the hypo-CPFEM and the hyper-CPFEM give identical stress predictions illustrates that both hypo-elasticity and hyper-elasticity are valid assumptions for crystal plasticity models of metals.
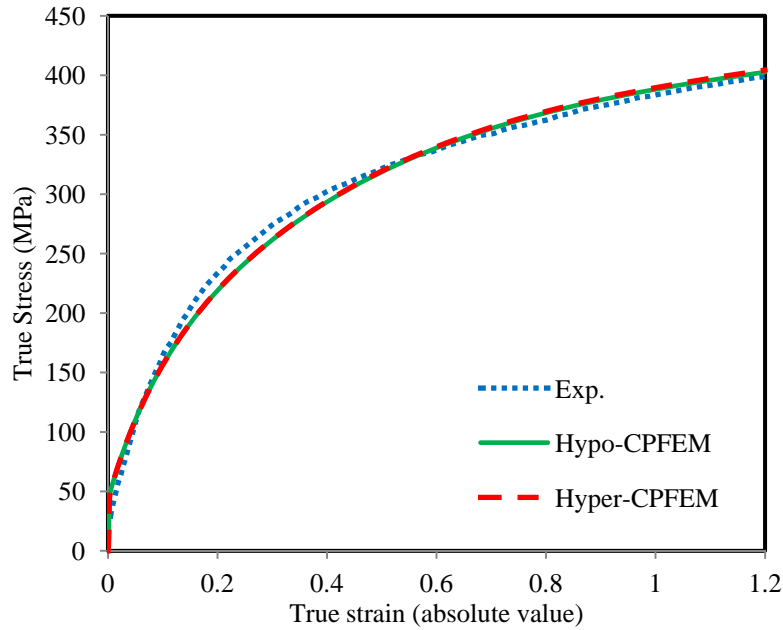

Fig. 3 Stress-strain curves from CPFEM simulations and experiment.

Table 2 CPU time for the simulations using two CPFEM models.

Problem time (s)	Hypo-CPFEM (s)	Hyper-CPFEM (s)
140	12580	13971

4.2. Rolling texture prediction

For the rolling simulation, periodic boundary conditions were applied on all faces of the RVE. The RVE was compressed along the z-axis with a speed of 0.02 mm/s to a thickness reduction of 70%. It was allowed to move along the x-axis freely while the deformation along the y-direction was constrained. The Euler angles after deformation in all integration points were output into files, and the orientation distribution function (ODF) were computed using the series expansion method with $l_{max} = 22$ and $\psi_0 = 7.5°$.

Fig. 4 shows the ODFs predicted by both hypo-CPFEM and hyper-CPFEM after rolling to 70% thickness reduction, while the corresponding CPU times are shown in Table 3. The ODF shows a typical rolling texture of FCC metals made of Brass, Goss, S, and Copper texture components [18] which qualitatively validates the correctness of the texture updating algorithms employed. Furthermore, the ODFs from the two simulations show excellent agreement with each other. It is reminded that the texture is updated by the tensor $\mathbf{R}^e$ which is obtained from the polar decomposition of the elastic deformation gradient tensor in the hyper-CPFEM. However, $\mathfrak{R}$ which is updated using $\mathbf{W}^*$ is employed for updating the texture in the hypo-CPFEM. The excellent agreement between the texture predictions demonstrates that both texture updating methods are equally accurate. Similar to the uniaxial compression case, the hypo-CPFEM is slightly faster (~10%) than the hyper-CPFEM, as shown in Table 3.

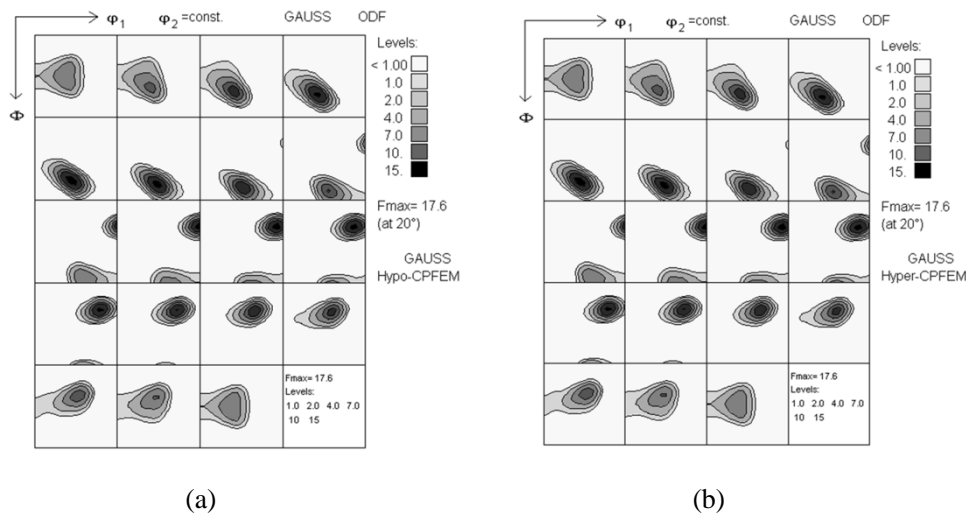

(a)   (b)

Fig. 4 Orientation distribution function (ODF) after 70% thickness reduction in rolling predicted by (a) hypo-CPFEM, (b) hyper-CPFEM.

Table 3 CPU time for rolling using two CPFEM models.

Problem time (s)	Hypo-CPFEM (s)	Hyper-CPFEM (s)
70	14581	16223

5. Conclusion

(1) A new forward Euler integration scheme is proposed for rate-dependent crystal plasticity, which employs the additive decomposition of the velocity gradient and uses a hypo-elasticity formulation for the stress calculation. The RDCP model with the new integration scheme has been implemented into the commercial finite element code LS-DYNA.

(2) This implementation is validated by comparison with a hyper-elastic formulation through two numerical tests. It is shown that the hypo-CPFEM is accurate for stress predictions, and the

numerical algorithm for updating texture is validated by comparison to hyper-CPFEM predictions.

(3)   Comparison of predictions by the hypo-CPFEM and by the hyper-CPFEM shows that the two models have equal accuracy when predicting stress and texture while the hypo-CPFEM is slightly more efficient.

(4)   Finally, the current forward Euler integration method, and thereby the hypo-CPFEM, can be further improved without loss of accuracy, through e.g. sub-stepping; this is part of an on-going work.

References

[1] TAYLOR G I. Plastic strain in metals [J]. Journal of Institute of Metals, 1938, 62: 307–324.

[2] DUMOULIN S, HOPPERSTAD O S, BERSTAD T. Investigation of integration algorithms for rate-dependent crystal plasticity using explicit finite element codes [J]. Computational Materials Science, 2009(4), 46: 785-799.

[3] ROTERS F, EISENLOHR P, HANTCHERLI L, TJAHJANTO D D, BIELER T R, RAABE D. Overview of constitutive laws, kinematics, homogenization and multiscale methods in crystal plasticity finite-element modeling: Theory, experiments, applications [J]. Acta Materialia, 2010, 58(4): 1152-1211.

[4] CHENG Li-dong, WANG Zhen-long. Scale effect mechanism on micro rod upsetting deformation analyzed by crystal plasticity model [J]. Transactions of Nonferrous Metals Society of China, 2012, 22(10): 2444-2450.

[5] LI Sai-yi. Application of crystal plasticity modeling in equal channel angular extrusion [J]. Transactions of Nonferrous Metals Society of China, 2013, 23(1): 170-179.

[6] VAN HOUTTE P. A comprehensive mathematical formulation of an extended Taylor–Bishop–Hill model featuring relaxed constraints, the Renouard–Wintenberger theory and a strain rate sensitivity model [J]. Textures and Microstructures, 1989, 8–9: 313–350.

[7] DELANNAY L, KALIDINDI S R, VAN HOUTTE P. Quantitative prediction of textures in aluminium cold rolled to moderate strains [J]. Materials Science and Engineering: A, 2002, 336(1-2): 233-244.

[8] ZHANG H, DONG X, WANG Q, ZENG Z. An effective semi-implicit integration scheme for rate dependent crystal plasticity using explicit finite element codes [J]. Computational Materials Science, 2012, 54: 208-218.

[9] PEIRCE D, ASARO R J, NEEDLEMAN A. An analysis of nonuniform and localized deformation in ductile single crystals [J]. Acta Metallurgica, 1982, 30(6): 1087-1119.

[10] LING X, HORSTEMEYER M F, POTIRNICHE G P. On the numerical implementation of 3d rate-dependent single crystal plasticity formulations [J]. International Journal for Numerical Methods in Engineering, 2005, 63(4): 548-568

[11] KUCHNICKI S N, CUITIÑO A M, RADOVITZKY R A. Efficient and robust constitutive integrators for single-crystal plasticity modeling [J]. International Journal of Plasticity, 2006, 22(10): 1988-2011.

[12] LI H W, YANG H, SUN Z C. A robust integration algorithm for implementing rate dependent crystal plasticity into explicit finite element method [J]. International Journal of Plasticity, 2008(2), 24: 267-288.

[13] KUCHNICKI S N, RADOVITZKY R A, CUITIÑO A M. An explicit formulation for multiscale modeling of bcc metals [J]. International Journal of Plasticity, 2008, 24(12): 2173-2191

[14] GRUJICIC M, BATCHU S. Crystal plasticity analysis of earing in deep-drawn OFHC copper cups [J]. Journal of Materials Science, 2002, 37(4): 753-764.

[15] HALLQUIST J O. LS-DYNA Keyword User's Manual Version 971 [M]. California: Livermore Software Technology Corporation, 2007.

[16] BELYTSCHKO T, LIU W K, MORAN B. Nonlinear Finite Elements for Continua and Structures [M]. New York: John Wiley, 2000.

[17] BUCHHEIT T E, WELLMAN G W, BATTAILE C C. Investigating the limits of polycrystal plasticity modeling [J]. International Journal of Plasticity, 2005, 21(2): 221-249.

[18] KOCKS U F, TOMÉ C N, WENK H R. Texture and Anisotropy: Preferred Orientations in Polycrystals and their effect on Materials Properties [M]. Cambridge: Cambridge University Press, 2000.

[19] KALIDINDI S R, BRONKHORST C A, ANAND L. Crystallographic texture evolution in bulk deformation processing of fcc metals [J]. Journal of the Mechanics and Physics of Solids, 1992, 40(3): 537-569.